Petroleum Science 23 (2026) 5836–5852

Contents lists available at ScienceDirect

Petroleum Science

journal homepage: www.keaipublishing.com/en/journals/petroleum-science

Original Paper

Multi-party collaboration: Enhancing the resilience of multi-energy logistics systems under demand uncertainty

Yong-Tu Liang [a,b,*], Guang-Tao Fu [a], Hao-Chong Li [a], Ren-Fu Tu [a], Xiao-Chen Gong [b], Yan-Ling Zhou [b], Rui Qiu [a], Lin Wang [a]

[a] Beijing Key Laboratory of Urban Oil and Gas Distribution Technology, China University of Petroleum (Beijing), Beijing, 102249, China
[b] Beijing University of Chemical Technology, Beijing, 100029, China

ARTICLE INFO

Article history:
Received 2 February 2026
Received in revised form
30 March 2026
Accepted 28 June 2026
Available online 3 July 2026

Edited by Meng-Jiao Zhou

Keywords:
Energy logistics systems
System resilience
Refined oil
New energy
Multi-party collaboration
Rolling robust simulation
Demand uncertainty

ABSTRACT

The global low-carbon transition is driving refining enterprises to shift from oil-dominant production toward diversified production, requiring the collaborative allocation of refined oil and new energy. However, logistics systems face significant challenges arising from nonlinear demand fluctuations and external disturbances, which traditional static approaches fail to address effectively. To this end, this study proposes a multi-party collaborative framework for multi-energy logistics systems. Specifically, a hybrid demand forecasting model integrating variational mode decomposition and bidirectional long short-term memory is developed to capture demand fluctuation characteristics. Based on the forecasting results, a multi-product, multi-modal rolling robust simulation model is constructed to dynamically balance economic benefits and system resilience under uncertainty. The proposed framework is validated through a case study of a large Chinese petrochemical enterprise, and a multi-dimensional evaluation method incorporating resilience, economic, environmental and energy indicators is proposed. The results show that: (i) compared with the deterministic scheme, the proposed simulation scheme increases operating costs by 3.64% under high volatility scenarios, while improving service level by 3.18%, reducing average stockout duration by 29.5%, and decreasing stockout quantity by 46.15%; (ii) the optimized energy product structure achieved by the model reduces carbon emissions by 7.7% and increases calorific value by 7.6%; and (iii) the study reveals integrated refinery and new energy configurations enabled by multi-party collaboration, providing quantitative support for enhancing system resilience. Based on these findings, policy implications are proposed to promote the development of energy logistics systems.

1. Introduction

The global shift toward a low-carbon energy mix, coupled with stringent decarbonization mandates, is fundamentally reconfiguring the operational paradigms of the traditional petrochemical sector. In the past decade, the global annual demand for refined oil has fluctuated between 0.9 and 1.4 billion tons (Liu et al., 2025). With the deepening of industrialization and breakthroughs in new energy technology, according to the International Energy Agency (IEA), the demand for refined oil is projected to peak before 2030. Simultaneously, the demand for chemical feedstocks and new energy shows a strong trend of continuous growth. By 2060, their aggregate demand is expected to increase to 13.8–20.8 billion tons of standard coal equivalents, accounting for 53%–71% of primary energy, replacing fossil energy as the main type of energy development (Popoola et al., 2026). Consequently, refining enterprises are adopting energy transition strategies, with "oil to chemicals" being the most prevalent approach. This strategy facilitates the pivotal transition of traditional refining capacity toward the production of high-value chemical feedstocks and emerging energy carriers (Akah et al., 2025). Leveraging the spatial compatibility between existing refined oil logistics and new energy logistics, the industry can directly utilize the surplus transportation capacity of

* Corresponding author.
E-mail address: liangyt21st@163.com (Y.-T. Liang).
Peer review under the responsibility of China University of Petroleum (Beijing).

https://doi.org/10.1016/j.petsci.2026.06.049
1995-8226/

refined oil to transport new energy. This strategy effectively avoids the excessive operating costs of constructing new infrastructure while mitigating the risk of asset idleness (Fu et al., 2025). However, the realization of this multi-party collaboration faces multifaceted challenges. Primarily, the collaboration necessitates a dynamic trade-off between the competing profitability of traditional refined oil and new energy. In addition, the inherent spatial mismatch between supply and demand for new energy necessitates large-scale, long-distance transfers. This extensive logistical process inevitably introduces transport time lags. Consequently, these lags render the system highly susceptible to demand volatility and external shocks, such as geopolitical conflicts (Zhang et al., 2025a). The inherent non-linearity of these fluctuations makes precise forecasting exceptionally difficult, thereby hampering proactive resource allocation. Despite these critical challenges, current research remains confined to independent, single-energy simulations, leaving a gap in multi-party collaborative operations that effectively balance economic benefits and system resilience.

Based on the above background, this study is motivated by three critical challenges:

(1) **Difficulty in characterizing uncertainty boundaries for resilience:** The demand for refined oil and new energy exhibits high nonlinear fluctuations driven by multiple factors. Current methodologies struggle to precisely quantify these uncertainty boundaries, leading to operational plans that frequently deviate from real-world conditions. Such misalignment results in either inventory surpluses or supply deficits, thereby undermining overall system resilience.
(2) **Lack of simulation models for balancing resilience and economy:** A complex dynamic trade-off exists between economic benefits and system resilience. Existing research lacks an adaptive collaboration approach to re-optimize operational plans in response to demand shifts. Consequently, decision-makers lack the tools to identify optimal strategies that harmonize cost-effectiveness with multi-party coordination.
(3) **Absence of quantitative metrics for multi-party collaborative resilience:** Multi-party collaboration involves conflicting goals and competing interests. However, a multi-dimensional evaluation method to quantitatively assess collaborative performance is still missing. This void precludes a scientific evaluation of whether an operational scheme achieves the necessary equilibrium between economic benefits and system resilience.

The contributions of this work are summarized as follows:

(1) A multi-party collaborative framework is proposed to govern multi-energy logistics resilience. By mapping demand uncertainty to parameter sets, it provides a structured approach to validate system effectiveness across diverse stochastic scenarios.
(2) A rolling robust simulation model is developed, coupling rolling horizon strategy with robust optimization. This approach synchronizes production and allocation, generating operation schemes that inherently buffer against demand uncertainty.
(3) The strategic coordination between refining and logistics stakeholders is quantified. Through a multi-dimensional evaluation method, the study provides empirical evidence of the synergy gains in resilience, as well as economic, environmental, and energy performance.
(4) This work reveals strategic policy implications for the energy transition. It offers a rigorous basis for calibrating the trade-off between economic premiums and the necessity of resilience buffers, guiding decision-makers toward adaptive energy shifts.

The remainder of this paper is structured as follows. Section 2 provides a comprehensive review of the technologies pertinent to resilience enhancement in logistics systems. Building upon this, Section 3 characterizes the research problem and delineates the integrated conceptual framework. Section 4 details the core mathematical formulations, comprising the hybrid demand forecasting model, rolling robust simulation model, and evaluation method. Section 5 then implements a real-world case study, followed by Section 6, which presents the simulation results and analyses to validate the model's efficacy, explores critical trade-offs, and derives targeted policy implications for enhancing system resilience. Finally, Section 7 concludes the paper by synthesizing the key findings and suggesting directions for future inquiry.

2. Literature review

2.1. Time-series prediction algorithm

To achieve the multi-party collaboration, accurate demand forecasting acts as the cornerstone for decision-making. Early research primarily relied on statistical methodologies such as the autoregressive integrated moving average model and its variants (Pasari and Shah, 2020). Characterized by structural simplicity and strong statistical interpretability, these models have been widely applied to relatively stable energy consumption forecasting. However, they typically rely on the assumption that time series are linear or can be rendered stationary via differencing (Kontopoulou et al., 2023). Consequently, they struggle to capture abrupt structural changes and complex non-linear dynamics, which leads to a substantial degradation in predictive accuracy under highly volatile market conditions. With the advancement of artificial intelligence, machine learning approaches represented by support vector regression (SVR) and artificial neural networks have gradually superseded traditional statistical models. Notably, recurrent neural networks and their advanced variant, long short-term memory (LSTM) networks, have demonstrated superior performance in processing time series data due to unique gating mechanisms that effectively address long-term dependencies. Meng et al. (2022a, 2022b) developed a highly accurate SVR-Markov Chain hybrid model for forecasting China's total energy consumption and structural evolution, significantly outperforming traditional methods and prior studies, providing a scientific basis for the 14th Five-Year Plan. Muzaffar et al. (2019) trained an LSTM network on electrical load data incorporating exogenous variables to perform multi-horizon forecasting. Despite these advantages, single deep learning models applied directly to raw high-noise data often fail to distinguish between underlying structural trends and stochastic noise. This limitation frequently results in overfitting or convergence to local optima, thereby constraining forecasting robustness. To address these challenges, the “decomposition-ensemble” strategy has emerged as a prominent research focus. The core premise of this strategy involves utilizing signal decomposition techniques to break down complex raw series into multiple sub-sequences characterized by singular frequencies and distinct features which are then individually forecasted and aggregated. Specifically, variational mode decomposition formulates the decomposition process as a non-recursive variational optimization problem (Dragomiretskiy and Zosso, 2013). This approach enables adaptive and effective signal separation while significantly mitigating mode mixing, thereby demonstrating superior noise immunity and decomposition precision.

2.2. Dynamic optimization and rolling horizon strategies

While accurate prediction provides the data foundation, the realization of multi-party collaboration requires dynamic adaptability in execution strategies. Traditional logistics simulation models are mostly deterministic models, meaning that a determined optimal plan is formulated for the entire cycle at the beginning of the planning period. Although these models are easy to solve, their applicability in the background of energy transition is poor. They assume that throughout the planning period, both the production plan on the refinery side and the transportation plan on the transport side are certain, which is seriously inconsistent with reality (Xiong et al., 2025). In actual operation, once facing sudden external disturbances, a conversion scheme and transportation scheme that are seemingly optimal at the beginning of the month may become completely unenforceable by the middle of the month due to the impact of external uncontrollable factors. To overcome the problem of poor adaptability of static plans, the rolling horizon strategy has been widely introduced into dynamic optimization research (Homsi et al., 2024). Rolling horizon decomposes the entire long planning period into a series of linked short periods. At each decision point, the model re-optimizes based on the latest information currently mastered, and then as time goes on, constantly updates the optimization interval and repeats this optimization process. Li et al. (2023) aimed at the coupling problem of chemical production and supply chain, proposed a multi-horizon optimization framework combining parameter prediction, and realized real-time operation response under supply chain fluctuations. Fattahi and Govindan (2020) developed a data-driven rolling horizon method to design a resilience distribution network under disruption risks, verifying the effectiveness of this strategy in supply chain dynamic reconfiguration. These studies fully prove the universality and superiority of the rolling horizon strategy as a dynamic optimization strategy in dynamically correcting various operating parameters of the system. However, when applying the rolling horizon strategy, existing studies often limit their optimization focus to the immediate response of a single logistics system, ignoring the complex dynamic trade-off between economic benefits and system resilience in the uncertain environment of energy transition.

2.3. Uncertainty programming and robust optimization

In the problem of multi-party collaboration optimization of multimedium petrochemical integrated logistics system under the background of energy transition, uncertain factors mainly come from the shrinkage of refined oil demand after peaking (Qiu et al., 2022), the nonlinear growth of converted product demand, and sudden disturbances from the external environment (Li et al., 2026). How to effectively deal with these uncertainties is the core difficulty of decision optimization. Compared with stochastic programming's strong dependence on probability distribution, robust optimization provides a more robust modeling paradigm. It does not need to know the exact probability density function of uncertain parameters, but instead finds the optimal solution that is still feasible under all possible worst-case scenarios within the set by constructing an uncertainty set (Huang and Wan, 2026). In numerous application studies, robust optimization has been proven to effectively improve the resilience of energy systems. For example, Selerio et al. (2022) developed a robust mixed-integer linear programming model to configure a multi-generation production system, effectively dealing with the uncertainty caused by supply chain disruptions and price fluctuations, ensuring system robustness under different emission policies. To address the multi-dimensional uncertainty in energy networks, Bai et al. (2025) proposed a quantum-inspired robust optimization method, successfully coordinating the scheduling problem where renewable energy generation and load demand fluctuate simultaneously. In addition, in the field of downstream supply chain, Awan et al. (2025) simulated disruption scenarios and verified the significant effect of robust optimization strategies in improving the resilience of downstream oil supply chains and minimizing costs. However, existing studies often focus on worst-case scenario protection in a single link when dealing with uncertainty challenges, while ignoring how to dynamically balance the uncertainty caused by refinery transformation and the cost premium caused by excessive conservatism of robust control in the long-period rolling decision process.

2.4. Summary and research gaps

Despite the significant advancements in the above-mentioned fields, several critical research gaps remain to be addressed:

(1) While the decomposition-ensemble strategy has improved forecasting accuracy, existing literature often treats demand prediction and logistics optimization as decoupled processes. There is a lack of approaches to effectively translate forecasting uncertainty intervals into actionable logistics decision boundaries.
(2) Most rolling horizon applications focus on single-energy systems. There is a lack of research that integrates the refinery conversion side with the multi-modal transportation side under a unified collaborative framework to address the dual-uncertainty of refined oil demand shrinkage and new energy growth.
(3) Current robust optimization models often prioritize worst-case protection, leading to excessive conservatism and high-cost premiums. A dynamic logic that balances economic performance with the strategic necessity of a resilience buffer has yet to be fully established.

Consequently, there is an urgent need for a rolling robust simulation approach that can bridge these gaps by synchronizing multi-party collaboration with resilience enhancement.

3. Methodology

3.1. Problem description

The global energy landscape is in a period of profound structural transition, marking a leap from traditional fossil fuel dominance to a new energy system, urgently requiring the construction of a multi-energy logistics system. As shown in Fig. 1, this logistics system covers four core sides: the refinery side, the depot side, the transportation side, and the customer side. Both refineries and oil depots are equipped with storage facilities to serve as essential logistical buffers. The sides are tightly coupled through four transportation modes: pipeline, waterway, railway, and highway, constructing a complex logistics network to ensure efficient material transportation between different nodes (Qiu et al., 2024a). As the supply node of the system, the refinery side has the functions of refined oil supply and material conversion, enabling the shift in production structure from refined oil to various converted energy products through different process routes. Specifically, the crude oil

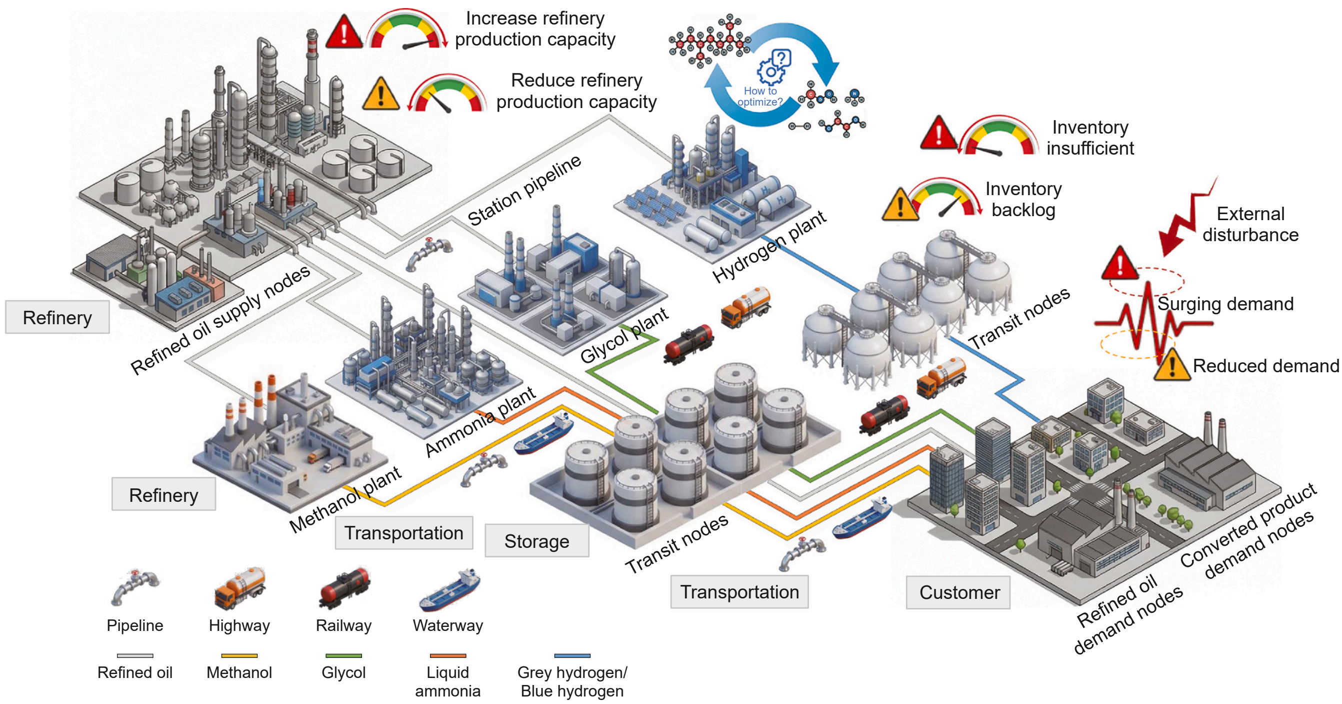

Fig. 1. Schematic diagram of multi-energy logistics systems.

processing flow can be divided into three conversion paths. The light components are mainly used to produce gasoline, or are converted into intermediates like ethylene and propylene through cracking and reforming processes, and then synthesized into ethylene glycol. The medium components yield diesel and kerosene while enabling the production of lubricating base oils through hydrocracking (Ge et al., 2023). The heavy components, in addition to producing heavy fuel oil and asphalt, undergo deep conversion via gasification or coking to generate methanol, liquid ammonia (Tu et al., 2024), and clean energy carriers such as grey and blue hydrogen. Furthermore, the system is continuously exposed to uncertain external environmental disturbances during operation, resulting in varying degrees of demand fluctuation at the customer end, which rapidly propagates to the production end via interconnected nodes (Shi et al., 2025). When market demand surges, the inventory volume at the depot side drops rapidly, necessitating an adjustment in the product conversion ratio at the refinery side to prioritize the supply of high-demand products. Conversely, a drop in demand leads to inventory accumulation, prompting a strategic shift in the product conversion ratio to minimize holding costs. Therefore, under demand uncertainty and capacity constraints, logistics system resilience depends on the ability to formulate efficient dynamic strategies.

3.2. Multi-party collaborative framework

Fig. 2 shows the multi-party collaborative framework for multi-energy logistics systems. The framework consists of three core modules: uncertainty quantification, rolling robust simulation, and R&3E (Resilience, Economy, Environment and Energy) evaluation and decision analysis. These modules interact closely to form a continuous data and decision-making loop. First, the uncertainty quantification module establishes the analytical foundation. For traditional refined oil, which possesses abundant historical data, the VMD-BiLSTM model is utilized to accurately capture their nonlinear demand trends and calculate prediction error intervals. Conversely, for converted new energy products, which are currently in a rapid growth phase with limited historical data accumulation, their uncertainty boundaries are determined by establishing demand fluctuation ranges. This module generates diverse simulation scenarios with varying fluctuation amplitudes based on empirical data characteristics. Second, the rolling robust simulation module serves as the computational core. Receiving the aforementioned disturbance boundaries as inputs, this module integrates robust optimization theory with a rolling horizon strategy to dynamically generate logistics schemes. At the mathematical level, it employs an uncertainty budget to identify integrated logistics schemes capable of withstanding worst-case scenarios within the predefined parameter sets. At the strategic level, the rolling horizon strategy is used to solve the problem of long-period dynamic adjustment. As shown in Fig. 2, the planning cycle is decomposed into a series of sliding time windows (t, $t+1$, …). At each decision moment, the model re-optimizes based on the latest system status and updated demand information, executes only the decision of the current window, and then the time window rolls forward and starts a new round of optimization. This iterative logic ensures that the generated logistics scheme can be dynamically corrected and respond in real-time according to environmental changes. Finally, the R&3E evaluation and decision analysis module assesses the holistic performance of the proposed schemes. The logistics schemes generated by the simulation module are sequentially fed into this evaluation module. By establishing a multi-dimensional evaluation method covering resilience, economy, environment and energy, this module utilizes empirical data from a large petrochemical enterprise to conduct a quantitative comparative analysis. The results validate the framework's effectiveness in calibrating the trade-off between economic benefits and system resilience, providing rigorous decision support for industrial practitioners. The evaluation outcomes act as a feedback mechanism. This mechanism dynamically quantifies the trade-offs between economic costs and system resilience. Based on these insights, decision-makers can adjust the uncertainty budget tolerance or alter the initial supply-demand configurations of the system.

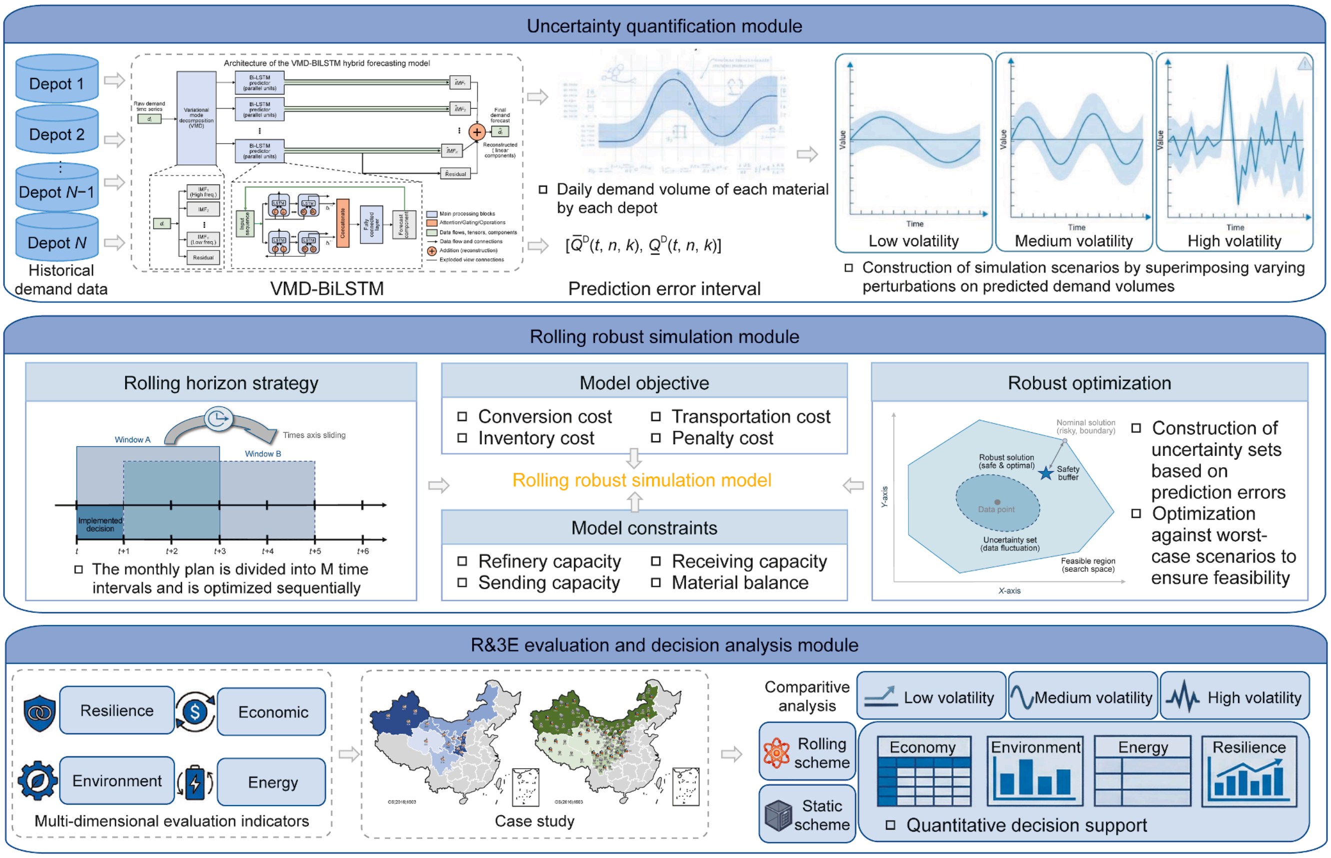

Fig. 2. The multi-party collaborative framework for multi-energy logistics systems.

4. Mathematical model

Let $T = \{1, 2, ..., t_{\max}\}$ denote the set of all time points, indexed by t. Let T_L denote the set of all time periods, where a time period t is composed of the consecutive time points t and $t+1$. Let $S = \{1, 2, ..., s_{\max}\}$ denote the set of all supply nodes, indexed by s. Let $H = \{1, 2, ..., h_{\max}\}$ denote the set of all transit nodes, indexed by h. Let $D = \{1, 2, ..., d_{\max}\}$ denote the set of all demand nodes, indexed by d. Let $N = \{1, 2, ..., n_{\max}\}$ denote the set of all nodes, indexed by n, where $N = S \cup H \cup D$. Let $M = \{1, 2, ..., m_{\max}\}$ denote the set of all transportation modes, indexed by m. Let $O = \{1, 2, ..., o_{\max}\}$ denote the set of all refined oil, indexed by o. Let $P = \{1, 2, ..., p_{\max}\}$ denote the set of all converted energy products, indexed by p. Let $K = \{1, 2, ..., k_{\max}\}$ denote the set of all refined oil and converted energy products, indexed by k, where $K = O \cup P$.

4.1. VMD-BiLSTM

It should be noted that the forecasting module is introduced in this study not as the primary methodological contribution, but as a supporting component to provide reliable demand fluctuation estimates for the subsequent uncertainty quantification and rolling robust simulation.

4.1.1. VMD

In a multimedium petrochemical integrated logistics system, directly applying data-driven prediction models to raw demand series often leads to unstable learning performance and limited robustness. To mitigate these issues, VMD is adopted as a preprocessing technique to decompose depot demand time series into multiple subcomponents with improved stationarity and clearer temporal structures.

Let $x_{t,n,k}$ denote the observed demand of product k at node n and time point t in the energy logistics system. The objective of VMD is to decompose the original demand series $x_{t,n,k}$ into a finite set of J intrinsic mode functions (IMFs), denoted by $\left\{u^j_{t,n,k}\right\}_{j=1}^{J}$, and a residual component $r_{t,n,k}$, such that each IMF captures oscillatory demand behavior around a specific center frequency. The decomposition satisfies the following reconstruction relationship:

$$x_{t,n,k} = \sum_{j=1}^{J} u^j_{t,n,k} + r_{t,n,k} \tag{1}$$

Unlike recursive signal decomposition approaches, VMD formulates the demand decomposition process as a constrained variational optimization problem. Each IMF is assumed to be an amplitude-modulated and frequency-modulated signal with limited bandwidth, representing demand fluctuations at a specific temporal scale. The bandwidth of each component is quantified by the squared L_2-norm of the gradient of its analytic signal after frequency shifting. The variational problem seeks to minimize the total bandwidth of all IMFs under the reconstruction constraint:

$$\min_{\{u^j\},\{\omega^j\}} \sum_{j=1}^{J} \left\| \partial_t \left[\left(\delta(t) + \frac{a}{\pi t} \right) * u_{t,n,k}^j \right] \mathrm{e}^{-a\omega^j t} \right\|_2^2$$
$$\text{s.t.} \sum_{j=1}^{J} u_{t,n,k}^j = x_{t,n,k} \tag{2}$$

where ω^j represents the center frequency of the k-th IMF, $\delta(t)$ is the Dirac delta function, and * denotes the convolution operator. By introducing a quadratic penalty factor and a Lagrange multiplier, the constrained optimization problem is transformed into an unconstrained form and solved iteratively using the alternating direction method of multipliers. This formulation enables stable convergence and effectively mitigates the mode-mixing problem that often arises in traditional decomposition methods.

From the perspective of logistics systems, the IMFs extracted by VMD correspond to demand fluctuations at different temporal scales. High-frequency components typically reflect short-term disturbances such as abrupt demand changes and rapid inventory adjustments, whereas low-frequency components capture long-term structural trends associated with seasonal demand patterns, production planning cycles, and energy transition dynamics. The residual term $r_{t,n,k}$ represents the remaining slowly varying trend that cannot be adequately described by the finite set of IMFs.

After decomposition, each component $u_{t,n,k}^j$ exhibits reduced non-stationarity and lower structural complexity compared with the original series $x_{t,n,k}$. This property significantly facilitates the learning process of subsequent prediction models and enhances forecasting robustness under uncertain operating conditions. Accordingly, all IMFs and the residual component are retained and separately used as inputs to the BiLSTM basic prediction model, forming the basis for accurate demand forecasting in the energy logistics system.

4.1.2. BiLSTM

After the VMD model, the oil depot demand series in energy logistics systems is represented by a set of intrinsic mode functions (IMFs) and a residual component, each exhibiting reduced non-stationarity and clearer temporal characteristics (Li et al., 2025). To capture the nonlinear temporal dependencies embedded in these decomposed demand components, a bidirectional long short-term memory network is employed as the prediction model. Let $u_{t,n,k}^j$ denote the k-th decomposed demand component of product k at oil depot n and time point t. In the forward direction, the LSTM updates its internal state sequentially according to the standard gating mechanism, where the forget gate, input gate, and output gate are given by:

$$f_t = \sigma\left(W_f h_{t-1} + U_f u_{t,n,k}^j + b_f\right) \tag{3}$$

$$n_t = \sigma\left(W_n h_{t-1} + U_n u_{t,n,k}^j + b_n\right) \tag{4}$$

and the candidate cell state is computed as:

$$\tilde{c}_t = \tanh\left(W_c h_{t-1} + U_c u_{t,n,k}^j + b_c\right) \tag{5}$$

The cell state is then updated by:

$$c_t = f_t \odot c_{t-1} + n_t \odot \tilde{c}_t \tag{6}$$

while the output gate and hidden state are obtained as:

$$y_t = \sigma\left(W_y h_{t-1} + U_y u_{t,n,k}^j + b_y\right) \tag{7}$$

$$\overrightarrow{h_{t,n,k}^j} = y_t \odot \tanh(c_t) \tag{8}$$

where $\sigma(\cdot)$ denotes the sigmoid activation function and $\odot$ represents element-wise multiplication. In parallel, a backward LSTM processes the same input sequence in reverse temporal order, yielding the backward hidden state $\overleftarrow{h_{t,n,k}^j}$. The forward and backward hidden states are concatenated to form the bidirectional representation.

$$h_{t,n,k}^j = \left[\overrightarrow{h_{t,n,k}^j} + \overleftarrow{h_{t,n,k}^j}\right] \tag{9}$$

which is subsequently mapped through a fully connected output layer to obtain the predicted value of the decomposed demand component, expressed as:

$$\hat{u}_{t,n,k}^j = W_h h_{t,n,k}^j + b_h \tag{10}$$

This prediction procedure is applied independently to all IMFs and the residual component, and the final point forecast of oil depot demand is reconstructed by linear superposition as:

$$\hat{x}_{t,n,k} = \sum_{j=1}^{J} \hat{u}_{t,n,k}^j + r_{t,n,k} \tag{11}$$

By jointly exploiting forward and backward temporal dependencies, the BiLSTM model provides an effective data-driven approach for modeling oil depot demand dynamics within energy logistics systems.

4.1.3. Data normalization and evaluation metrics

Data normalization is a critical preprocessing step for demand forecasting in energy logistics systems, as it transforms input variables into a consistent numerical scale and alleviates the adverse effects caused by large magnitude differences among features. In practical oil depot operations, the outbound demand volumes of different oil products often exhibit substantial variability across depots and time periods, which may lead to numerical instability during deep learning model training and hinder effective parameter optimization. Normalization helps stabilize the training process, accelerates convergence, and enhances the robustness and generalization capability of the prediction model. In this study, the Min–Max normalization method is adopted to rescale all input variables into the interval [0, 1], which is expressed as Eq. (12).

$$\hat{X}_{\mathrm{n}} = \frac{X_{\mathrm{n}} - X_{\min}}{X_{\max} - X_{\min}} \tag{12}$$

where X_{n} denotes the original input value, $\hat{X}_{\mathrm{n}}$ represents the normalized value, and $X_{\min}$ and $X_{\max}$ correspond to the minimum and maximum values of the input dataset, respectively. After model prediction, the normalized outputs are transformed back to their original scale to enable direct comparison with observed demand values.

To quantitatively evaluate the forecasting performance of the proposed demand prediction model, several widely used evaluation metrics are employed. The root mean square error (RMSE), mean absolute error (MAE), and mean absolute percentage error (MAPE) are adopted to measure prediction accuracy from different perspectives, where lower values indicate smaller deviations between predicted and observed demand. Collectively, these metrics provide a comprehensive and reliable assessment of the accuracy and effectiveness of the proposed oil depot demand forecasting model.

4.2. Multi-product, multi-modal rolling robust simulation model

4.2.1. Objective function

The multi-product, multi-modal rolling robust simulation model aims to reduce the total cost of the four segments of transportation, conversion, storage and stockout in the multi-energy logistics system. Eq. (13) represents the objective function *FLG*, which includes transportation cost *FTC*, conversion cost *FCC*, storage cost *FSC*, and stockout penalty cost *FPC*. *FTC* represents the cost of shipping refined oil from refineries to all depots and from transit depots to all depots. *FCC* represents the cost required to convert one product into another. *FSC* represents the cost required for holding refined oil and converted energy products at refineries, transit depots, and regular depots. In addition, *FPC* represents the penalty for unmet demand at transit depots and regular depots. From the perspective of specific interest relationships among different stakeholders, this multi-party collaboration is mathematically formulated under a centralized optimization mechanism, which inherently constitutes a cooperative game theory framework. Unlike a non-cooperative game where individual entities greedily minimize their isolated costs (Fan et al., 2024), the cooperative framework integrates all participants into a unified global objective function (Eq. (13)). As indicated in comparative analyses of energy logistics (Tu et al., 2024), variations toward non-cooperative relationships typically induce higher marginal friction costs and lower overall system resilience. Therefore, managing this network from a globally centralized perspective ensures that different nodes collaboratively share inventory buffers and material conversion capacities, overcoming individual barriers to achieve an optimal operational state for the entire multi-energy logistics system.

$$\min FLG = FTC + FCC + FSC + FPC \tag{13}$$

$$\begin{aligned} FTC = & \sum_{t\in T_L}\sum_{n\in S}\sum_{n'\in H\cup D}\sum_{m\in M}\sum_{k\in K} c^{\mathrm{qv}}_{n,n',m,k} Q^{\mathrm{V}}_{t,n,n',m,k} \\ & + \sum_{t\in T_L}\sum_{n'\in H}\sum_{n''\in H\cup D}\sum_{m\in M}\sum_{k\in K} c^{\mathrm{qv}}_{n',n'',m,k} Q^{\mathrm{V}}_{t,n',n'',m,k} \end{aligned} \tag{14}$$

$$FCC = \sum_{t\in T_L}\sum_{n\in S\cup H}\sum_{k\in O}\sum_{k'\in P} c^{\mathrm{qc}}_{n,k,k'} Q^{\mathrm{C}}_{t,n,k,k'} \tag{15}$$

$$FSC = \sum_{t\in T}\sum_{n\in S}\sum_{k\in K} c^{\mathrm{qu}}_{n,k} Q^{\mathrm{U}}_{t,n,k} + \sum_{t\in T}\sum_{n'\in H\cup D}\sum_{k\in K} c^{\mathrm{qu}}_{n',k} Q^{\mathrm{U}}_{t,n',k} \tag{16}$$

$$FPC = \sum_{t\in T}\sum_{n\in H\cup D}\sum_{k\in K} c^{\mathrm{qi}}_{n,k} Q^{\mathrm{I}}_{t,n,k} \tag{17}$$

4.2.2. Model constraints

(1) Refinery capacity constraint

Eq. (18) ensures that the refined oil and converted product planned production volume $Q^{\mathrm{X}}_{t,n,k}$ at these refineries is equal to the planned production sampling volume $q^{\mathrm{x}}_{t,n,k}$. Eq. (19) ensures that the refined oil and converted product inventory volume $Q^{\mathrm{U}}_{t,n,k}$ at these refineries does not exceed the maximum inventory volume $q^{\mathrm{u,max}}_{t,n,k}$ and not is less than the minimum inventory volume $q^{\mathrm{u,min}}_{t,n,k}$. Eq. (20) ensures that the total inventory volume of refined oil and converted energy products at these refineries does not exceed the maximum collaborative capacity $q^{\mathrm{cou,max}}_{n,k}$.

$$Q^{\mathrm{X}}_{t,n,k} = q^{\mathrm{x}}_{t,n,k} \quad \forall t\in T_{\mathrm{L}}, n\in S, k\in K \tag{18}$$

$$q^{\mathrm{u,min}}_{n,k} \le Q^{\mathrm{U}}_{t,n,k} \le q^{\mathrm{u,max}}_{n,k} \quad \forall t\in T, n\in S, k\in K \tag{19}$$

$$\sum_{k\in K} Q^{\mathrm{U}}_{t,n,k} \le \sum_{k\in K} q^{\mathrm{cou,max}}_{n,k} \quad \forall t\in T, n\in S \tag{20}$$

(2) Refinery conversion constraint

Eq. (21) represents the constraint for the transfer-out of refined oil products. It ensures that the refined oil supply volume $Q^{\mathrm{R}}_{t,n,k}$, together with the cumulative sum of refined oil transfer-out volume $\sum_{k'\in P} Q^{\mathrm{C}}_{t,n,k,k'}$, is less than or equal to the refined oil planned production volume $Q^{\mathrm{X}}_{t,n,k}$. Eq. (22) represents the constraint for the transfer-in of conversion products. It ensures that the converted product supply volume $Q^{\mathrm{R}}_{t,n,k}$ is less than or equal to the cumulative sum of converted product transfer-in volume $\sum_{k'\in O} \gamma_{n,k',k} \cdot Q^{\mathrm{C}}_{t,n,k',k}$ and the converted product planned production volume $Q^{X}_{t,n,k}$.

$$Q^{\mathrm{R}}_{t,n,k} + \sum_{k'\in P} Q^{\mathrm{C}}_{t,n,k,k'} \le Q^{\mathrm{X}}_{t,n,k} \quad \forall t\in T_L, n\in S, k\in O \tag{21}$$

$$Q^{\mathrm{R}}_{t,n,k} \le \sum_{k'\in O} \gamma_{n,k',k} \cdot Q^{\mathrm{C}}_{t,n,k',k} + Q^{\mathrm{X}}_{t,n,k} \quad \forall t\in T_L, n\in S, k\in P \tag{22}$$

(3) Sending synergistic capacity constraint

Eq. (23) ensures that the transportation volume $\sum_{n'\in H\cup D}\sum_{k\in K} Q^{\mathrm{V}}_{t,n,n',m,k}$ from a refinery or transit depot using transportation modes within a unit time period is less than the maximum collaborative sending capacity $q^{\mathrm{covs,max}}_{n,m}$. This constraint reflects the upper bound of loading and dispatching capability at transit depots and regular depots under multi-modal transportation.

$$\sum_{n'\in H\cup D}\sum_{k\in K} Q^{\mathrm{V}}_{t,n,n',m,k} \le q^{\mathrm{covs,max}}_{n,m} \quad \forall t\in T_L, n\in S\cup H, m\in M \tag{23}$$

(4) Receiving synergistic capacity constraint

There are constraints on the volume received by regular depots or transit depots via different transportation modes within a unit time period (Zhang et al., 2025b). Eq. (24) ensures that the sum of the received volume $\sum_{n'\in S\cup H}\sum_{k\in K} Q^{\mathrm{V}}_{t,n',n,m,k}$ from refineries and transit depots, together with the in-transit transportation volume $\sum_{n''\in S\cup H}\sum_{k\in K}Q^{Z}_{t,n'',n,m,k}$ at the planning cutoff, is less than the depot's maximum collaborative receiving capacity $q^{\text{covr,max}}_{n,m}$.

$$\sum_{n'\in S\cup H}\sum_{k\in K}Q^{V}_{t,n',n,m,k}+\sum_{n''\in S\cup H}\sum_{k\in K}Q^{Z}_{t,n'',n,m,k}\le q^{\text{covr,max}}_{n,m}\quad \forall t\in T_L, n\in H\cup D, m\in M \tag{24}$$

(5) Depot capacity constraint

Eq. (25) ensures that the refined oil inventory volume $Q^{U}_{t,n,k}$ at these depots does not exceed the maximum inventory volume $q^{\text{u,max}}_{n,k}$ and is not less than the minimum inventory volume $q^{\text{u,min}}_{n,k}$. This constraint is used to maintain the inventory level of each product within the allowable operating range. Eq. (26) ensures that the total inventory volume of refined oil and converted energy products at these depots does not exceed the maximum collaborative capacity $q^{\text{cou,max}}_{n,k}$. This constraint reflects the overall inventory limitation of the depot in collaborative logistics operation.

$$q^{\text{u,min}}_{n,k}\le Q^{U}_{t,n,k}\le q^{\text{u,max}}_{n,k}\quad \forall t\in T, n\in H\cup D, k\in K \tag{25}$$

$$\sum_{k\in K}Q^{U}_{t,n,k}\le\sum_{k\in K}q^{\text{cou,max}}_{n,k}\quad \forall t\in T, n\in H\cup D \tag{26}$$

(6) Material balance constraint

Eqs. (27)–(29) are the material balance constraints for refineries (Qiu et al., 2024b). At the initial time, the inventory volume of each refinery $Q^{U}_{t=0,n,k}$ is equal to its initial inventory volume. During each time period, the inventory volume $Q^{U}_{t+1,n,k}$ is determined by the inventory volume $Q^{U}_{t,n,k}$ at the previous time point, plus the supply volume $Q^{R}_{t,n,k}$, minus the product transfer-out volume for conversion $\sum_{k'\in P}Q^{C}_{t,n,k,k'}$, plus the converted product transfer-in volume $\sum_{k'\in O}\gamma_{n,k',k}\cdot Q^{C}_{t,n,k',k}$, and minus the transportation volume $\sum_{n'\in H\cup D}\sum_{m\in M}Q^{V}_{t,n,n',m,k}$.

$$Q^{U}_{t=0,n,k}=q^{\text{u,ini}}_{n,k}\quad \forall n\in S, k\in K \tag{27}$$

$$Q^{U}_{t+1,n,k}=Q^{U}_{t,n,k}+Q^{R}_{t,n,k}-\sum_{k'\in P}Q^{C}_{t,n,k,k'}+\sum_{k'\in O}\gamma_{n,k',k}\cdot Q^{C}_{t,n,k',k}-\sum_{n'\in H\cup D}\sum_{m\in M}Q^{V}_{t,n,n',m,k}\quad \forall t\in T_L, n\in S, k\in K \tag{28}$$

$$Q^{U}_{t=0,n,k}=q^{\text{u,ini}}_{n,k}\quad \forall n\in H\cup D, k\in K \tag{29}$$

(7) Robust material balance constraint

Eq. (30) represents the uncertainty expression of the demand variable $\tilde{Q}^{D}_{\tau,n,k}$, which embeds random demand fluctuation into the rolling robust simulation model in the form of a nominal value $\overline{Q}^{D}_{\tau,n,k}$ and a disturbance term $\xi_{t,n,k}\cdot\hat{Q}^{D}_{t,n,k}$. The range of values for the disturbance variable $\xi_{t,n,k}$ is from 0 to 1. At the theoretical formulation level, this study adopts the widely recognized robust optimization framework proposed by Bertsimas and Sim (2004) to construct the uncertainty sets (Bertsimas and Sim, 2004). Eq. (31) is the robust material balance constraint for transit depots and regular depots under demand uncertainty. During each time period, the cumulative available volume at the depot side must be no less than the cumulative uncertain demand. Specifically, the left-hand side represents the net material availability at the current time period. It is determined by the current inventory volume $Q^{U}_{\tau,n,k}$, minus the inventory volume $Q^{U}_{\tau+1,n,k}$ at the next time point, plus the stockout volume $Q^{I}_{\tau,n,k}$ in the current time period, plus the received transportation volume $\sum_{n'\in S\cup H}\sum_{m\in M}Q^{V}_{\tau,n',n,m,k}$ in the current time period, plus the in-transit transportation volume $\sum_{n''\in S\cup H}\sum_{m\in M}Q^{Z}_{\tau,n'',n,m,k}$ in the current time period, minus the transportation volume $\sum_{n'''\in H\cup D}\sum_{m\in M}Q^{V}_{\tau,n,n''',m,k}$ in the current time period. The right-hand side represents the cumulative demand requirement under the robust counterpart, which is composed of the nominal demand value $\sum_{\tau=1}^{t}\overline{Q}^{D}_{\tau,n,k}$ and the robust protection terms. Specifically, the robust protection terms include the term associated with the uncertainty budget $\Gamma_{n,k}\cdot\pi_{n,k}$, together with the auxiliary dual variables corresponding to the deviations of the uncertain demand $\sum_{\tau=1}^{t}\rho_{\tau,n,k}$ in each time period. Eqs. (32)–(34) define the corresponding relationships for the dual variables $\pi_{n,k}$ and $\rho_{\tau,n,k}$ and their non-negativity constraints

The introduction of the uncertainty budget $\Gamma_{n,k}$ implies the assumption that it is historically and spatially improbable for the worst-case extreme demand peaks to occur simultaneously across all consumer nodes at every time period. By restricting the total number of active worst-case deviations through $\Gamma_{n,k}$, the model effectively mimics the spatial-temporal correlation and stochastic nature of energy market disturbances, avoiding the physical impossibility of absolute global disruption. Because directly solving this infinite worst-case scenario maximization within a constraint is computationally intractable, strong duality theory of linear programming is explicitly applied to transform the structural formulation (Meng et al., 2022a, 2022b). By constructing the dual problem of the inner parameter maximization block, the intractable component is strictly converted into an equivalent minimization problem. During this transition, the dual variables $\pi_{n,k}$ and $\rho_{\tau,n,k}$ are introduced to replace the original disturbance variables. Specifically, $\pi_{n,k}$ acts as the dual variable associated with the uncertainty budget limit, representing the marginal penalty of increasing the robustness level; conversely, $\rho_{\tau,n,k}$ corresponds to the individual upper bounds of each disturbance variable, absorbing the specific deviation peaks.

$$\tilde{Q}^{D}_{t,n,k}=\overline{Q}^{D}_{t,n,k}+\xi_{t,n,k}\cdot\hat{Q}^{D}_{t,n,k}\quad \forall t\in T, n\in D, k\in K \tag{30}$$

$$\sum_{\tau=1}^{t}\left(Q^{U}_{\tau,n,k}-Q^{U}_{\tau+1,n,k}+Q^{I}_{\tau,n,k}+\sum_{n'\in S\cup H}\sum_{m\in M}Q^{V}_{\tau,n',n,m,k}+\sum_{n''\in S\cup H}\sum_{m\in M}Q^{Z}_{\tau,n'',n,m,k}-\sum_{n'''\in H\cup D}\sum_{m\in M}Q^{V}_{\tau,n,n''',m,k}\right)\ge\sum_{\tau=1}^{t}\overline{Q}^{D}_{\tau,n,k}+\Gamma_{n,k}\cdot\pi_{n,k}+\sum_{\tau=1}^{t}\rho_{\tau,n,k}\ \forall t\in T, n\in D, k\in K \tag{31}$$

$$\pi_{n,k}+\rho_{\tau,n,k}\geq\widehat{Q}^{\mathrm{D}}_{\tau,n,k}\quad\forall\tau\in\{1,2,...,t\},n\in D,k\in K\tag{32}$$

$$\pi_{n,k}\geq 0\quad\forall n\in D,k\in K\tag{33}$$

$$\rho_{\tau,n,k}\geq 0\quad\forall\tau\in\{1,2,...,t\},n\in D,k\in K\tag{34}$$

4.3. Multi-dimensional evaluation method

The goal of multi-energy logistics systems is not only to complete the physical transportation of refined oil and converted energy products, but more importantly, to ensure the continuous service of downstream refined oil and converted energy products to the consumer market, to mitigate uncertainty from the demand side. Therefore, evaluating this logistics system requires a multi-dimensional evaluation method, covering four dimensions: resilience, economy, environment and energy. Resilience evaluation indicators include average stockout duration, stockout quantity, and service level. The economic evaluation indicator is operation cost. The environmental evaluation indicator is carbon emission. The energy consumption evaluation indicator is calorific value.

(1) Average stockout duration

The average stockout duration evaluation (RAS) indicator aims to measure the average stockout duration of the system by calculating the arithmetic mean of the stockout days of each oil depot in the logistics system within the planning cycle, thereby evaluating the overall degree of impact on that system when facing supply interruptions.

$$R^{\mathrm{RS}}_{t,n,k}=\begin{cases}1, & \text{if }\left(\sum\limits_{n'\in S\cup H}\sum\limits_{m\in M}Q^{\mathrm{V}}_{t,n',n,m,k}+Q^{\mathrm{U}}_{t,n,k}-\tilde{Q}^{\mathrm{D}}_{t,n,k}\right)<0\\ 0, & \text{otherwise}\end{cases}\tag{35}$$

$$\mathrm{RAS}=\frac{\sum\limits_{t\in T_L}\sum\limits_{n\in H\cup D}\sum\limits_{k\in K}R^{\mathrm{RS}}_{t,n,k}}{K}\tag{36}$$

(2) Stockout quantity

The stockout quantity evaluation indicator (RSQ) is used to quantify the scale of total demand that failed to be met within the planning cycle. When the available quantity of a certain demand node (composed of planned receiving quantity and existing inventory quantity) is lower than its actual demand quantity, it is determined that a stockout occurs. This indicator intuitively reflects the degree of shortage of refined oil and converted energy products by accumulating the stockout quantity.

$$\mathrm{RSQ}=\sum_{t\in T_L}\sum_{n\in H\cup D}\sum_{k\in K}\max\left\{0,\tilde{Q}^{\mathrm{D}}_{t,n,k}-\left(\sum_{n'\in S\cup H}\sum_{m\in M}Q^{\mathrm{V}}_{t,n',n,m,k}+Q^{\mathrm{U}}_{t,n,k}\right)\right\}\tag{37}$$

(3) Service level

The service level evaluation indicator (RSL) is defined as the proportion of the satisfied demand to the total demand (i.e., the net value after utilizing total demand volume minus stockout quantity, divided by total demand volume), which is used to measure the extent to which the system successfully achieves supply–demand matching.

$$\mathrm{RSL}=\frac{\sum\limits_{t\in T_L}\sum\limits_{n\in H\cup D}\sum\limits_{k\in K}\left(\dfrac{\tilde{Q}^{\mathrm{D}}_{t,n,k}-\max\left\{0,\tilde{Q}^{\mathrm{D}}_{t,n,k}-\left(\sum\limits_{n'\in S\cup H}\sum\limits_{m\in M}Q^{\mathrm{V}}_{t,n',n,m,k}+Q^{\mathrm{U}}_{t,n,k}\right)\right\}}{\tilde{Q}^{\mathrm{D}}_{t,n,k}}\right)}{K}\tag{38}$$

(4) Operation cost

The operation cost evaluation indicator (EOC) quantifies the total cost of the entire system within the planning cycle. This indicator is composed of three main parts: transportation cost, conversion cost, and storage cost. Transportation cost is the transport expense of various materials using different transport modes, conversion cost is the expense of converting refined oil into converted energy products, and storage cost is the holding expense of each node.

$$\begin{aligned}\mathrm{EOC}=&\sum_{t\in T_L}\sum_{n\in S}\sum_{n'\in H\cup D}\sum_{m\in M}\sum_{k\in K}c^{\mathrm{qv}}_{n,n',m,k}Q^{\mathrm{V}}_{t,n,n',m,k}\\&+\sum_{t\in T_L}\sum_{n'\in H}\sum_{n''\in H\cup D}\sum_{m\in M}\sum_{k\in K}c^{\mathrm{qv}}_{n',n'',m,k}Q^{\mathrm{V}}_{t,n',n'',m,k}\\&+\sum_{t\in T_L}\sum_{n\in S\cup H}\sum_{k\in O}\sum_{k'\in P}c^{\mathrm{qc}}_{n,k,k'}Q^{\mathrm{C}}_{t,n,k,k'}+\sum_{t\in T}\sum_{n\in S}\sum_{k\in K}c^{\mathrm{qu}}_{n,k}Q^{\mathrm{U}}_{t,n,k}\\&+\sum_{t\in T}\sum_{n'\in H\cup D}\sum_{k\in K}c^{\mathrm{qu}}_{n',k}Q^{\mathrm{U}}_{t,n',k}\end{aligned}\tag{39}$$

(5) Carbon emission

The carbon emission evaluation indicator (ECE) measures the potential carbon emissions avoided by the system through conversion strategies within the planning cycle. Specifically, since a portion of refined oil is transferred out for chemical production through conversion operations instead of being directly consumed as fuel, this indicator quantifies the total consumer-side carbon emissions that would have originally been produced if this refined oil were burned as fuel.

$$\mathrm{ECE}=-\sum_{t\in T_L}\sum_{n\in S\cup H}\sum_{k\in O}\sum_{k'\in P}e^{\mathrm{carb}}_{n,k}\cdot Q^{\mathrm{C}}_{t,n,k,k'}\tag{40}$$

(6) Calorific value

The calorific value evaluation indicator (ECV) is used to evaluate the calorific value capability of chemical products obtained by the system through material conversion strategies within the planning cycle. Specifically, this indicator quantifies the total calorific value contained in the newly added chemical products transferred in through conversion operations, intuitively reflecting the increment in the system's chemical energy reserves.

$$\mathrm{ECV}=\sum_{t\in T_L}\sum_{n\in S\cup H}\sum_{k\in O}\sum_{k'\in P}e^{\mathrm{calo}}_{n,k'}\cdot\gamma_{n,k,k'}\cdot Q^{\mathrm{C}}_{t,n,k,k'}\tag{41}$$

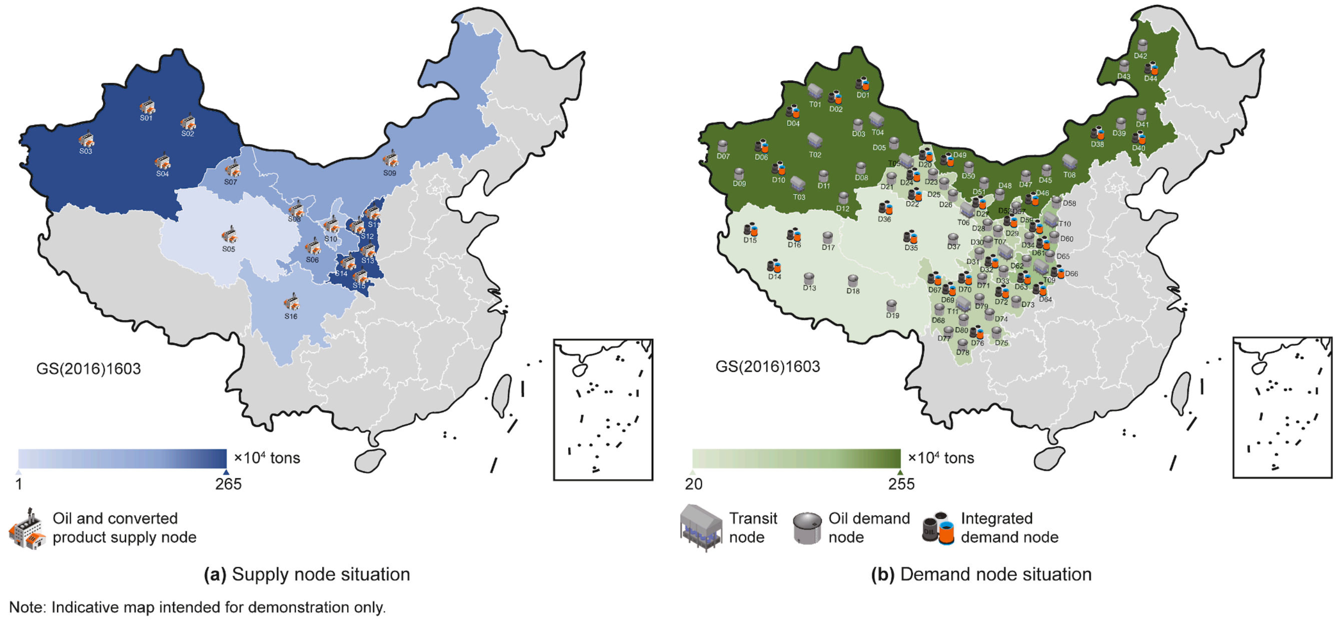

Fig. 3. Schematic diagram of the system node distribution.

5. Case study

This paper takes the multi-energy logistics system of a large petrochemical enterprise in China as a case study. This case involves 20 distinct materials (O01–O20), comprising 15 refined oil products (diesel and gasoline) and 5 converted energy products, namely ethylene glycol, methanol, liquid ammonia, grey hydrogen and blue hydrogen. Fig. 3(a) shows the distribution locations of 16 supply nodes (S1–S16), and Fig. 3(b) shows the distribution locations of 11 transit nodes (T1–T11) and 80 demand nodes (D1–D80). Each supply node possesses supply and conversion functions. The demand nodes are divided into refined oil demand nodes and integrated demand nodes (consuming both refined oil and converted energy products). The spatial geographic distances between different nodes are logically determined based on actual route extraction from the Google Maps platform. Moreover, critical empirical parameters, including transportation route information, initial inventory volumes, target inventory volumes, supply and demand situation, are sourced directly from the petrochemical enterprise's logistics management system. In contrast, since converted energy products are still in the early stages of rapid market penetration with insufficient longitudinal data to train deep learning models, their nominal demands and fluctuation boundaries in this study are mapped based on the annual reports of the same enterprise, properly adjusted by the actual new energy development plans of different provinces. The monthly supply and demand situation in each region is represented by color depth, and addressing the mismatch of supply and demand of various products in geographical space needs to use 4 transportation modes (TRK, SHP, PIP, RAL) for resource deployment.

Table 1 summarizes the unit transportation costs of the four transportation modes, all preserving the average standard freight rates within the research area. Considering policy subsidies, equipment depreciation, actual operation, and other factors, it is assumed that the unit conversion cost is 1050 CNY/t, and the unit inventory cost of the depot is 10 CNY/t (Cai et al., 2025). Table 2 summarizes the material conversion ratios based on the element conservation method, without considering process losses, and relying solely on average carbon content to calculate the theoretical maximum output value (Tong et al., 2013). Taking converting input O01 to output O16 as an example, consuming 1 ton of O01 yields 0.49 tons of O16. Table 3 details the physicochemical parameters of each material (Ma et al., 2022; Tu et al., 2023). Taking material O01 as an example, its calorific value is 42.65 GJ/t. If consumed directly as fuel, the combustion of one ton of O01 would result in 3.17 t of CO_2 emissions.

The proposed rolling robust simulation model is coded in Python and solved using Gurobi Optimizer (version 11.0.2). The computation is executed on a computer equipped with a 13th Gen Intel Core i5-13600KF CPU (14 physical cores, 20 logical processors) and running the Windows 11 operating system. The constructed model possesses a massive scale, containing 432,997 variables (columns), 394,665 constraints (rows), and 995,861 non-zero coefficients. Despite its massive scale, thanks to the deterministic linear reformulation, the solver effectively resolved the problem and achieved the optimal objective within 5 s.

Table 1
Cost parameters of multi-modal transportation.

Mode	TRK	SHP	PIP	RAL
Transportation cost (CNY/ton-km)	0.68	0.17	0.15	0.30

6. Results and discussion

6.1. Prediction effect analysis

To provide a more robust and depot-independent evaluation of model performance, the prediction accuracy for the same oil product across the two depots is averaged corresponding to the 92#, the 95#, and the diesel, as summarized in Tables 4–6. This aggregation strategy mitigates site-specific fluctuations and highlights the intrinsic predictive capability of each model.

Across all oil products, the proposed model consistently outperforms the benchmark methods in terms of RMSE, MAE, and MAPE. For the 92# case, the proposed approach achieves an average RMSE of 56.68 and MAE of 43.09, which are approximately 70% lower than those of traditional machine learning models such as Backpropagation Neural Network (BP), Support Vector Regression (SVR), Random Forest (RF), and XGBoost. In contrast, the ARIMA

Table 2
Conversion ratio parameters among different materials.

Transfer-in material	Transfer-out materials	Ratio	Transfer-in material	Transfer-out materials	Ratio
O01–O07	O16	0.49	O08–O15	O16	0.73
	O17	2.29		O17	2.27
	O18	0.20		O18	0.20
	O19	0.20		O19	0.20
	O20	1.13		O20	1.13

Table 3
Carbon emission factors and calorific values of different materials.

Material	CO_2 emission, t CO_2/t	Calorific value, GJ/t	Material	CO_2 emission, t CO_2/t	Calorific value, GJ/t
O01	3.17	42.65	O11	3.08	43.30
O02	3.17	42.65	O12	2.93	42.00
O03	3.16	42.55	O13	2.93	42.00
O04	3.15	42.40	O14	2.95	42.20
O05	3.14	42.30	O15	3.10	43.50
O06	3.13	42.10	O16	0.00	19.10
O07	3.12	42.10	O17	1.37	19.90
O08	3.05	43.10	O18	0.00	120.00
O09	2.93	41.80	O19	0.00	120.00
O10	2.93	41.80	O20	0.00	18.60

Table 4
Average prediction accuracy for the 92# case (two depots).

Model	RMSE	MAE	MAPE
BP	192.303	137.337	18.438
SVR	204.481	152.405	20.191
ARIMA	2.998×10^6	2.059×10^6	175.756
RF	198.138	146.732	19.500
XGBoost	204.644	153.467	20.142
The proposed model	**56.676**	**43.092**	**5.630**

Table 5
Average prediction accuracy for the 95# case (two depots).

Model	RMSE	MAE	MAPE
BP	123.014	87.840	26.347
SVR	127.946	89.327	26.479
ARIMA	2.790×10^6	2.108×10^5	537.320
RF	130.112	91.606	27.894
XGBoost	129.323	92.295	28.012
The proposed model	**38.810**	**28.883**	**8.083**

Table 6
Average prediction accuracy for the diesel case (two depots).

Model	RMSE	MAE	MAPE
BP	278.993	214.001	29.879
SVR	282.924	215.256	30.533
ARIMA	289.371	220.450	30.819
RF	278.409	214.076	30.288
XGBoost	278.940	214.584	30.287
The proposed model	**88.534**	**66.933**	**8.993**

model exhibits severe performance degradation, reflected by extremely large error magnitudes, indicating its limited applicability in capturing the nonlinear and nonstationary demand dynamics of refined oil products. A similar performance pattern is observed for the 95# case. The proposed model reduces the average MAPE to 8.08%, whereas the compared methods generally exceed 26%. This substantial improvement demonstrates the proposed framework's enhanced capability in handling high volatility and low base-demand scenarios, where conventional models tend to suffer

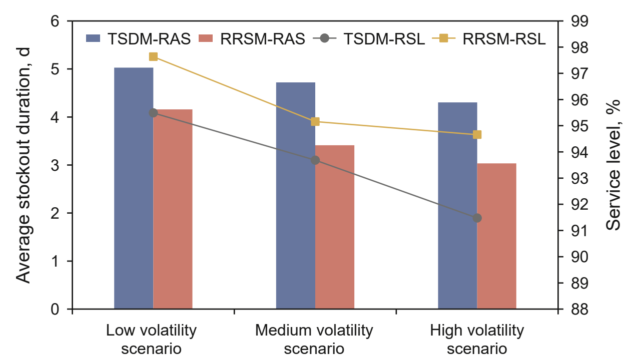

Fig. 4. Comparison of service level and average stockout duration between TSDM and RRSM.

from amplified relative errors. For the diesel case, which exhibits stronger seasonality and more pronounced demand inertia, the proposed model still maintains a clear advantage, achieving an average RMSE of 88.53 and MAPE of 8.99%. In comparison, all benchmark models yield MAPE values around 30%, suggesting that they struggle to simultaneously capture long-term trends and short-term fluctuations in diesel consumption.

Overall, the averaged results across depots confirm that the proposed model delivers stable and superior predictive performance across different oil products and demand characteristics. The consistent error reduction observed in all three cases indicates that the model's effectiveness is not confined to a specific depot or fuel type, thereby validating its robustness and generalization capability in multi-depot refined oil demand forecasting scenarios.

6.2. System resilience analysis

Fig. 4 shows the comparison results of the traditional static deterministic simulation model (TSDM) and the proposed multi-product, multi-modal rolling robust simulation model (RRSM) in terms of two resilience indicators, average stockout duration (RAS) and service level (RSL), under three different demand volatility scenarios. Under the low volatility scenario, the rolling model already shows better performance than the static model. The service level of the rolling model reached 97.63%, which is higher than the static model's 95.49%. Meanwhile, the average stockout duration of the rolling model is controlled at 4.16 days, significantly better than the static model's 5.03 days. These results suggest that the integration of the rolling horizon strategy and robust optimization theory enhances system resilience even within a comparatively stable operating environment. As the demand fluctuation intensifies from a low volatility scenario to a high volatility scenario, the superiority of the rolling model becomes more prominent. The service level of the static model shows a worsening trend as volatility increases, dropping from 95.49% under low volatility to 91.48% under high volatility, a decrease of about 4.01%. In contrast, the service level of the rolling model remains at 94.66% in the high volatility scenario, with a decrease of only about 2.97%. Especially in high volatility scenarios, the service level of the rolling model is 3.18% higher than that of the static model. Regarding the comparison of average stockout duration, the rolling model similarly demonstrates exceptional performance in accelerating recovery from stockout events. In all volatility scenarios, the average stockout duration of the rolling model is significantly lower than that of the traditional static model. In the high volatility scenario, the average stockout days for the static model are 4.30 days, while that of the rolling model is only 3.03 days, a reduction of about 1.27 days, a decrease of 29.5%.

To further analyze the feasibility of the operational schemes generated by the rolling model, Fig. 5 presents the daily shortage heatmaps for some demand nodes under the high volatility scenario. The rolling model effectively alters the spatiotemporal distribution of shortages. Specifically, the total stockout quantity under the static model scheme amounts to 82.51 $\times$ 10^4 tons, whereas the rolling model scheme effectively mitigates this figure to 44.43 $\times$ 10^4 tons, representing a significant reduction of 46.15%. Regarding the specific distribution patterns, stockouts in the static model exhibit characteristics of high intensity and long duration. After sustaining demand shocks at the beginning of the month, several depots (e.g., D40, D10, D46) not only experienced significant initial shortages but also showed repeated deep-colored shortage blocks in the middle and late month. Taking depot D40 as an example, under the static model scheme, it reached a peak shortage of 2.55 $\times$ 10^4 tons on the 18th, and still had a shortage of 1.08 $\times$ 10^4 tons on the 20th. In contrast, shortages in the rolling model are characterized by low intensity and fast recovery. The color blocks of the rolling model are significantly lighter and more dispersed, no longer forming continuous areas as in the static model. Taking depot D40 again, on the 18th when the static model had severe shortages, the operating scheme generated by the rolling model reduced the shortage to only 3.7 tons. This proves that the rolling model can rectify logistics schemes in a timely manner through the rolling horizon strategy and robust optimization theory, eliminating early shortage impacts and preventing further deterioration.

6.3. System economic analysis

Table 7 provides a detailed comparison of the various cost components between the static model and the rolling model under different volatility scenarios. Since the static model performs overall planning at the beginning of the month, its cost components remain unchanged in all scenarios, with a total cost of 64.49 $\times$ 10^8 CNY. In contrast, the total cost of the rolling model gradually increases as the volatility rises. In the high volatility scenario, the robust rolling model's total cost reaches 66.84 $\times$ 10^8 CNY, which is 3.64% higher than that of the static model. The rolling model copes with market fluctuations by increasing upstream material conversion inputs and holding more safety stock, which increases operating expenses but achieves higher system resilience. The Sankey diagram in Fig. 6 reveals the reasons for the cost differences from the perspectives of transport structure and resource flow. Leveraging an operational strategy of direct refinery dispatch coupled with material conversion, the system circumvents total reliance on transit depot redistributions during shortages. Instead, it utilizes the production capacity of adjacent refineries to synthesize required products for direct high-capacity delivery to demand nodes.

The traditional static model is frequently associated with excessive conservatism, typically resulting in unnecessarily high inventory holding costs to hedge against worst-case scenarios. However, the multi-party collaborative framework proposed in this study inherently mitigates this over-conservatism through the

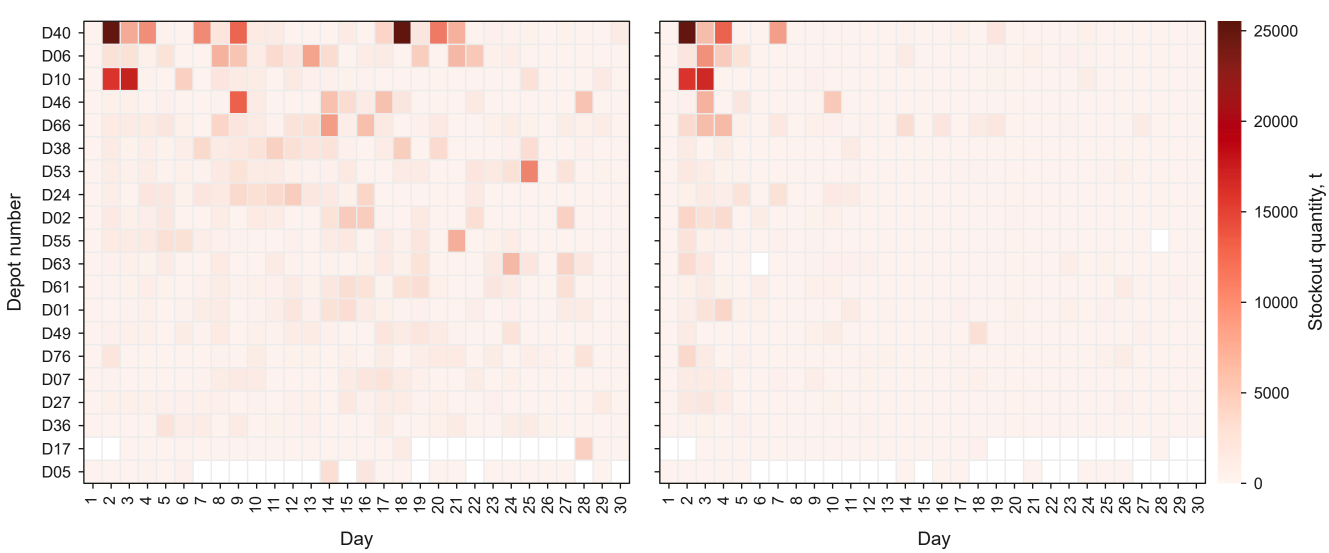

(a) Static model

(b) Rolling model

Fig. 5. Heatmap visualization of daily stockout quantities distribution under the severe fluctuation scenario.

Table 7
Economic performance analysis of TSDM and RRSM across three volatility scenarios.

Model	Costs, $\times 10^8$ CNY	Low volatility scenario	Medium volatility scenario	High volatility scenario
The traditional static model	Transportation	27.13	27.13	27.13
	Refinery inventory	0.46	0.46	0.46
	Depot inventory	0.43	0.43	0.43
	Conversion	36.48	36.48	36.48
	Total cost	64.49	64.49	64.49
The robust rolling model	Transportation	26.57	26.60	26.46
	Refinery inventory	0.54	0.66	0.82
	Depot inventory	0.12	0.11	0.13
	Conversion	37.40	39.15	39.43
	Total cost	64.63	66.52	66.84
Total cost comparison, %		0.22	3.15	3.64

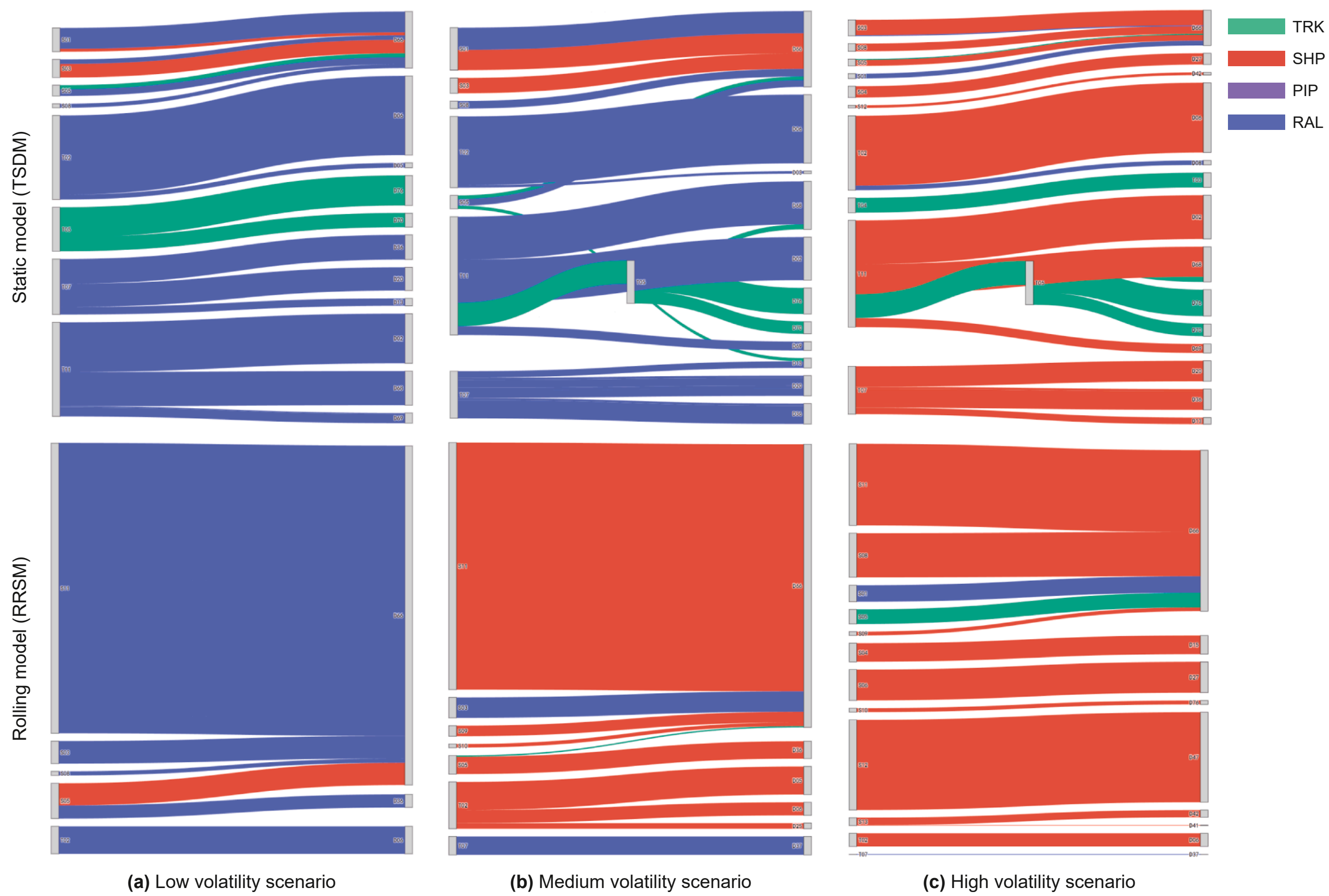

Fig. 6. Sankey diagrams illustrating the material flow structure difference under three volatility scenarios.

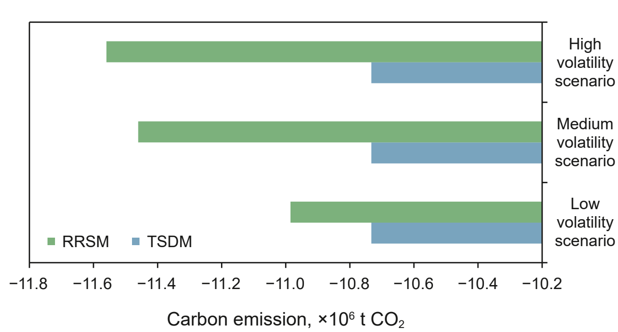

Fig. 7. Comparison of carbon emission evaluation indicator between TSDM and RRSM.

rolling horizon strategy. By continuously updating the real-time system status and adjusting the uncertainty boundaries at each rolling window, the system dynamically releases excess safety buffers when the forecasted extreme disruptions do not materialize, thus avoiding rigid, long-term cost premiums. The comparative analysis across the low, medium, and high volatility scenarios presented in Table 7 effectively functions as an evaluation of varying robustness settings. Rather than tuning a singular abstract mathematical budget parameter, calibrating the amplitude of the disturbance intervals across these three scenarios provides decision-makers with a more intuitive and operational understanding of how varying degrees of uncertainty intensity drive the dynamic trade-off between resilience gains and economic costs.

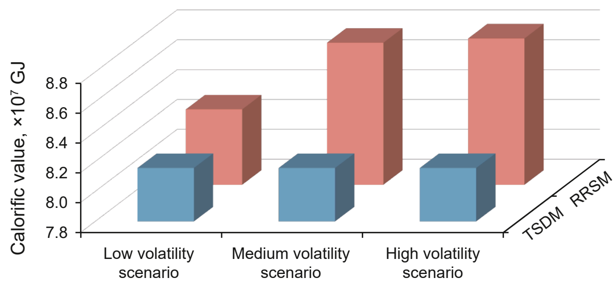

Fig. 8. Comparison of calorific value evaluation indicator between TSDM and RRSM.

6.4. System environment and energy analysis

This section evaluates the carbon emission and calorific value of the logistics schemes generated by the two models under different scenarios. Fig. 7 presents the comparison results of the carbon emission evaluation indicator (ECE) for the static model and the rolling model. The carbon emission evaluation indicator measures the potential carbon emissions avoided by the system through conversion strategies, where a larger absolute negative value indicates a greater reduction in potential emissions. Under the low volatility scenario, the rolling model has already shown better performance than the static model. However, as the demand fluctuation intensifies from the low volatility scenario to the high volatility scenario, the environmental advantages of the rolling model become increasingly significant. Due to its inherent static planning nature, the carbon emission evaluation indicator of the static model scheme remains constant across all volatility scenarios, staying at -10.73×10^6 t CO_2. In contrast, the carbon emission evaluation indicator of the rolling model scheme shows an optimization trend as volatility increases, reaching -10.99×10^6 t CO_2, -11.46×10^6 t CO_2, and -11.56×10^6 t CO_2 in the low, medium, and high volatility scenarios, respectively. Especially in the high volatility scenario, compared with the static model, the rolling model avoids an additional potential carbon emission of 0.83×10^6 t CO_2, achieving an improvement of about 7.7%. This indicates that the rolling model adopts a proactive strategy, increasing the conversion ratio of refined oil to chemical products and clean energy, achieving significant consumer-side carbon reduction effects.

Fig. 8 further presents the comparison results of the calorific value evaluation indicator (ECV). Consistent with the trend observed in the carbon emission indicator, the rolling model demonstrates similar performance in enhancing energy calorific value. The calorific value of the static model scheme is 8.16×10^7 GJ in all scenarios. The performance advantages of the rolling model become increasingly prominent as demand volatility escalates. Specifically, the calorific value of the rolling model scheme is 8.30×10^7 GJ in the low volatility scenario, then increases to 8.75×10^7 GJ in the medium volatility scenario, and finally reaches 8.78×10^7 GJ in the high volatility scenario. In the high volatility scenario, the calorific value of the rolling model scheme is 0.62×10^7 GJ higher than that of the static model scheme, achieving an energy calorific value growth of approximately 7.6%. This improvement confirms that the rolling model successfully achieved a strategic shift from single fuel supply to a diversified chemical energy reserve focus. By converting more fuel-attribute materials into feedstock-attribute chemical products, the rolling model effectively enhances the potential industrial value.

6.5. Ablation study

To rigorously justify the necessity of integrating the core methodological components, namely uncertainty quantification and the rolling horizon strategy, an ablation-style comparative analysis is conducted. Fundamentally, this analysis is constructed upon two methodological dimensions: the assumption of supply-demand parameters (Deterministic vs. Uncertain) and the execution strategy (Static vs. Rolling). The cross-combination of these dimensions theoretically yields four distinct operational paradigms: (1) the deterministic static model, (2) the deterministic rolling model, (3) the robust static model, and (4) the proposed rolling robust model. It is worth noting that for the deterministic rolling model, because the supply and demand parameters are strictly deterministic, the recursively updated system status identically matches the initial expectations. Consequently, it generates the exact same operational schemes and simulation results as the deterministic static model. Thus, it is conceptually acknowledged here but merged with the deterministic static model in the subsequent quantitative comparison.

As presented in Table 8, the evolution of resilience indicators across the distinct scenarios clearly demonstrates the specific contribution of each component. Taking the high volatility scenario as an example, the deterministic static model's service level sharply plummets to 91.48%, and the stockout quantity peaks at 82.51×10^4 tons. When robust optimization is introduced in isolation (the robust static model), the service level recovers to 93.09% and the stockout quantity drops to 66.92×10^4 tons. This improvement highlights the value of delineating uncertainty ranges to provide a proactive capacity buffer. Finally, when the rolling horizon strategy is fully integrated (the rolling robust model), the service level further surges to 94.66%, and the stockout quantity drastically decreases to 44.43×10^4 tons. This final performance leap substantiates that the dynamic rolling strategy can provide the temporal flexibility required to correct logistical

Table 8
Ablation analysis of system resilience under varying operational models and volatility scenarios.

Volatility scenario	Optimization model	Average stockout duration, d	Service level, %	Stockout quantity, $\times 10^4$ t
Low volatility	The deterministic static model	5.03	95.49	43.67
	The robust static model	4.74	95.95	39.21
	The proposed rolling robust model	4.16	97.63	22.91
Medium volatility	The deterministic static model	4.72	93.69	61.13
	The robust static model	3.66	94.24	55.74
	The proposed rolling robust model	3.41	95.16	43.53
High volatility	The deterministic static model	4.30	91.48	82.51
	The robust static model	3.54	93.09	66.92
	The proposed rolling robust model	3.03	94.66	44.43

misalignments and truncate average stockout durations (down to 3.03 days).

6.6. Policy implications

Based on the simulation findings, several policy implications are derived to facilitate the transition of the multi-energy logistics system. These recommendations aim to bridge the gap between theoretical modeling and industrial practice:

(1) Transition from static planning to dynamic collaborative planning

Logistics operators should move away from traditional monthly static planning in favor of rolling horizon strategies. Crucially, the functional silos between refining production and logistics transportation must be broken down. Establishing a multi-party collaborative protocol between the refining and logistics sectors is essential to proactively hedge against market volatility and systemic risks.

(2) Reconfigure performance evaluation based on R&3E evaluation

Decision-makers should move beyond narrow cost-centric metrics and adopt the R&3E evaluation system. Performance assessments should incorporate resilience indicators, including service levels and stockout durations, alongside environmental and energy metrics such as carbon emissions and calorific value. Incentivizing operators to accept manageable economic premiums in daily operations is vital to securing long-term systemic resilience and low-carbon benefits.

(3) Enhance structural flexibility and strategic redundancy

Case analysis demonstrates that refineries with resource conversion capabilities are pivotal in absorbing fluctuations. Strategic investments should be prioritized to enhance the energy conversion capability of process units at key nodes, enabling rapid transitions between refined oil and new energy. Furthermore, developing supporting storage infrastructure provides a necessary resilience buffer to mitigate extreme market disturbances.

7. Conclusions and future directions

7.1. Conclusions

As a critical hub for energy transition, the multi-energy logistics system is continuously exposed to uncertainty disturbances triggered by non-linear market demand fluctuations, which pose severe challenges to its operational continuity. Within this dynamic and high-risk environment, traditional static logistics planning methodologies are becoming obsolete, frequently resulting in low plan execution rates and supply-demand mismatches. Therefore, improving the ability of the logistics system to cope with uncertainty is crucial for ensuring economic benefits and system resilience. By constructing a multi-party collaborative framework for multi-energy logistics systems, this paper quantitatively evaluates the system performance across diverse uncertainty scenarios from four dimensions: resilience, economy, environment and energy.

The research results show that the multi-product, multi-modal rolling robust simulation model constructed in this paper performs excellently in non-economic evaluation dimensions. First, regarding resilience indicators, as demand fluctuation intensifies from low to high volatility, the advantage of the rolling model over the traditional static deterministic model becomes increasingly significant. In the high volatility scenario, the rolling model increases the service level by 3.18%, shortens the average stockout duration by 1.27 days, achieving a decrease of 29.5%, and reduces the stockout quantity by 38.08×10^4 tons, representing a decrease of 46.15%. Heatmap analysis further confirms that the rolling model successfully transforms the high-intensity and long-duration shortage pattern of the static model into a low intensity and fast recovery pattern. Second, in the environmental and energy aspects, under the high volatility scenario, the rolling model avoids about 0.83×10^6 t CO_2 of potential carbon emissions, achieving a 7.7% benefit improvement. Meanwhile, it increases the calorific value reserve by 0.62×10^7 GJ, improving the energy value by 7.6%. Finally, in the economic and resource allocation aspects, this improvement in resilience, environmental and energy benefits comes at a cost, mainly reflected in an increase in operating costs of about 3.64%. This shows that the model successfully converts uncontrollable uncertainty risk into controllable operating costs by increasing material conversion input and holding safety stock, thereby enhancing system resilience. Synthesizing the case study and research findings, this paper proposes policy implications for enhancing system resilience from the perspectives of energy logistics system managers and operators.

7.2. Limitations and future directions

This study constructs a multi-party collaborative framework for multi-energy logistics systems to balance economic benefits and system resilience under uncertainty. However, several limitations remain. First, this study focuses primarily on demand-side uncertainty, while uncertainties on the supply and logistics sides are not explicitly considered. Future research can develop collaborative logistics system simulation models incorporating multi-source uncertainties. Second, this study addresses multi-objective trade-offs by transforming uncertainty into cost minimization under constraints. Future work may adopt multi-objective optimization methods to generate Pareto frontiers and support decision-making under different risk preferences. Finally, as emerging energy demands continue to grow, logistics networks will become increasingly heterogeneous and complex. Future research can further investigate the coupling effects between multi-modal transportation networks and multi-energy carriers to support long-term energy transition.

CRediT authorship contribution statement

Yong-Tu Liang: Writing – review & editing, Writing – original draft, Validation, Methodology, Funding acquisition. **Guang-Tao Fu:** Writing – review & editing, Writing – original draft, Investigation. **Hao-Chong Li:** Writing – review & editing, Software, Data curation. **Ren-Fu Tu:** Visualization, Validation, Conceptualization. **Xiao-Chen Gong:** Supervision, Project administration, Investigation. **Yan-Ling Zhou:** Software, Data curation, Conceptualization. **Rui Qiu:** Methodology, Funding acquisition, Conceptualization. **Lin Wang:** Visualization, Resources, Investigation.

Declaration of competing interests

The authors declare the following financial interests/personal relationships which may be considered as potential competing interests: Yong-Tu Liang reports was provided by Foundation for Innovative Research Groups of the National Natural Science Foundation of China. If there are other authors, they declare that they have no known competing financial interests or personal

relationships that could have appeared to influence the work reported in this paper.

Acknowledgements

This work is supported by the National Natural Science Foundation of China (52502411). The authors are grateful to all study participants.

Appendix A. Supplementary data

Supplementary data to this article can be found online at https://doi.org/10.1016/j.petsci.2026.06.049.

Nomenclature

Parameters	
$c^{qu}_{n,k}$	Unit inventory cost of product k in node n, CNY/t
$c^{qi}_{n,k}$	Unit penalty cost of product k out of stock in node n, CNY/t
$c^{qc}_{n,k,k'}$	Unit conversion cost of transfer-out volume of product k to product k' in refinery n, t
$c^{qv}_{n,n',m,k}$	Unit transportation cost of product k from node n to node n' by transportation mode m, CNY/t
$q^{x}_{t,n,k}$	Planned production sampling volume of product k in node n at time period t, t
$q^{u,ini}_{n,k}$	Initial inventory volume of product k in node n, t
$q^{u,max}_{n,k}$ $q^{u,min}_{n,k}$	Maximum or minimum Inventory volume of product k in node n, t
$q^{cou,max}_{n,k}$	Maximum collaborative capacity of product k in node n, t
$q^{covs,max}_{n,m}$	Maximum collaborative sending capacity of transportation mode m in node n, t
$q^{covr,max}_{n,m}$	Maximum collaborative receiving capacity of transportation mode m in node n, t
$\gamma_{n,k',k}$	Material conversion ratio of product k to product k' in node n
$\Gamma_{n,k}$	Uncertain budget parameters of product k in node n
$\overline{Q}^{D}_{t,n,k}$	Nominal demand value of product k in node n at time period t, t
$\widehat{Q}^{D}_{t,n,k}$	Maximum allowed deviation of product k in node n at time period t, t
Decision variables	
$Q^{V}_{t,n,n',m,k}$	Transportation volume of product k sent from node n to node n' by transportation mode m at time period t, t
$Q^{Z}_{t,n,n',m,k}$	In-transit transportation volume of product k sent from node n to node n' by transportation mode m at time period t, t
$Q^{X}_{t,n,k}$	Planned production volume of product k in node n at time period t, t
$Q^{R}_{t,n,k}$	Supply volume of product k in node n at time period t, t
$Q^{C}_{t,n,k,k'}$	Transfer-out volume of product k to product k' in refinery n at time period t, t
$Q^{U}_{t,n,k}$	Inventory volume of product k in node n at time point t, t
$Q^{I}_{t,n,k}$	Stockout volume of product k in node n at time point t, t
$Q^{D}_{t,n,k}$	Demand volume of product k in node n at time period t, t
$\tilde{Q}^{D}_{t,n,k}$	Demand sampling volume of product k in node n at time period t, t
$\xi_{t,n,k}$	Uncertain disturbance variable of product k in node n at time period t, t

References

Akah, A.C., Al-Shafei, E., Xu, Q., et al., 2025. Direct catalytic cracking of crude oil-to-chemicals: Impact of steam catalytic cracking on petrochemicals yield. Chem. Eng. J. Adv. 23, 100794. https://doi.org/10.1016/j.ceja.2025.100794.

Awan, M.A.H., Naseem, A., Ahsan, A., et al., 2025. Evaluating disruption scenarios for improving downstream oil supply chain resilience and cost minimization using monte Carlo simulation. Sci. Rep. 15 (1). https://doi.org/10.1038/s41598-025-22678-9.

Bai, Y., Sui, Y., Deng, X., et al., 2025. Quantum-inspired robust optimization for coordinated scheduling of PV-hydrogen microgrids under multi-dimensional uncertainties. Sci. Rep. 15 (1). https://doi.org/10.1038/s41598-025-12280-4.

Bertsimas, D., Sim, M., 2004. The price of robustness. Oper. Res. 52 (1), 35–53. https://doi.org/10.1287/opre.1030.0065.

Cai, L.Y., Huang, M.Y., Yu, B., et al., 2025. Methanol-oil co-transportation system: Strategic facility planning for multiproduct pipelines to maximize benefits. J. Pipeline Sci. Eng., 100422 https://doi.org/10.1016/j.jpse.2025.100422.

Dragomiretskiy, K., Zosso, D., 2013. Variational mode decomposition. IEEE Trans. Signal Process. 62 (3), 531–544. https://doi.org/10.1109/TSP.2013.2288675.

Fan, W., Fan, Y., Yao, X., et al., 2024. Distributed transaction optimization model of multi-integrated energy systems based on nash negotiation. Renew. Energy 225, 120196. https://doi.org/10.1016/j.renene.2024.120196.

Fattahi, M., Govindan, K., 2020. Data-driven rolling horizon approach for dynamic design of supply chain distribution networks under disruption and demand uncertainty. Decis. Sci. J. 53 (1), 150–180. https://doi.org/10.1111/deci.12481.

Fu, G.T., Tu, R.F., Qiu, R., et al., 2025. Energy, economic and environmental impact analysis of adjusting oil refinery capacity: An interregional optimization approach for resource allocation. Energy 320, 135275. https://doi.org/10.1016/j.energy.2025.135275.

Ge, J.Q., Zhang, P., Sun, F.M., et al., 2023. Catalyst grading technology for promoting the diesel hydrocracking to naphtha. Pet. Sci. 20 (6), 3798–3806. https://doi.org/10.1016/j.petsci.2023.05.015.

Homsi, G., Gendron, B., Jena, S.D., 2024. Rolling horizon strategies for a dynamic and stochastic ridesharing problem with rematches. Discret. Appl. Math. 343, 191–207. https://doi.org/10.1016/j.dam.2023.10.016.

Huang, S.Y., Wan, Z., 2026. Learning uncertainty by constructing multi-box uncertainty sets from the datasets with complicated distributions: validated by robust optimization. Inf. Sci. 733, 122988. https://doi.org/10.1016/j.ins.2025.122988.

Kontopoulou, V.I., Panagopoulos, A.D., Kakkos, I., et al., 2023. A review of ARIMA vs. machine learning approaches for time series forecasting in data driven networks. Future Internet 15 (8), 255. https://doi.org/10.3390/fi15080255.

Li, H.R., Zhang, S.Y., Qiu, T., 2023. Receding horizon optimization of ethylene cracking operation and scheduling under supply chain fluctuations. Ind. Eng. Chem. Res. 62 (12), 5125–5140. https://doi.org/10.1021/acs.iecr.2c04366.

Li, H.Z., Shao, T.M., Gao, X., et al., 2025. Forecasting carbon price using a hybrid framework based on Bayesian optimization algorithm. Pet. Sci. 22 (12), 5314–5328. https://doi.org/10.1016/j.petsci.2025.10.010.

Li, Y., Hanif, M.W., Wen, M., et al., 2026. Geopolitical risks and the global renewable energy transition: implications for energy security and

economic resilience. Energy Rep. 15, 108875. https://doi.org/10.1016/j.egyr.2025.12.012.
Liu, J.Y., Guo, F.Q., Shi, Y., et al., 2025. Study on the evolutionary characteristics and robustness of the global refined oil trade network. Energy 331, 137032. https://doi.org/10.1016/j.energy.2025.137032.
Ma, Z.K., Cheng, L.M., Wang, Q.H., et al., 2022. Co-combustion characteristics and CO_2 emissions of low-calorific multi-fuels by TG-FTIR analysis. Energy 252, 123919. https://doi.org/10.1016/j.energy.2022.123919.
Meng, Y.Z., Chen, R.-R., Deng, T.H., 2022a. Two-stage robust optimization of power cost minimization problem in gunbarrel natural gas networks by approximate dynamic programming. Pet. Sci. 19 (5), 2497–2517. https://doi.org/10.1016/j.petsci.2021.09.048.
Meng, Z.S., Sun, H.K., Wang, X., 2022b. Forecasting energy consumption based on SVR and Markov model: A case study of China. Front. Environ. Sci. 10, 883711. https://doi.org/10.3389/fenvs.2022.883711.
Muzaffar, S., Afshari, A., 2019. Short-term load forecasts using LSTM networks. Energy Proc. 158, 2922–2927. https://doi.org/10.1016/j.egypro.2019.01.952.
Pasari, S., Shah, A., 2020. Time series auto-regressive integrated moving average model for renewable energy forecasting. In: Sangwan, K., Herrmann, C. (eds) Enhancing Future Skills and Entrepreneurship. https://doi.org/10.1007/978-3-030-44248-4_7.
Popoola, L.T., Nwogbu, C.C., Taura, U., et al., 2026. Achieving effective operations in petrochemical industries using affordable and clean energy: Techniques, benefits, barriers and solutions. Cleaner Waste Systems 13, 100453. https://doi.org/10.1016/j.clwas.2025.100453.
Qiu, R., Liang, Y.T., Liao, Q., et al., 2022. Primary logistics planning of oil products under the imbalance of supply and demand. Pet. Sci. 19 (4), 1915–1925. https://doi.org/10.1016/j.petsci.2022.03.021.
Qiu, R., Tu, R.F., Wei, X.M., et al., 2024a. Evaluation and optimization of pipeline pricing strategies on oil product logistics in China. J. Pipeline Sci. Eng. 4 (1), 100144. https://doi.org/10.1016/j.jpse.2023.100144.
Qiu, R., Zhang, B., Zhao, W., et al., 2024b. An integrated MINLP model for multi-party coordination in downstream oil supply chain. Pet. Sci. 21 (3), 2066–2079. https://doi.org/10.1016/j.petsci.2023.12.008.
Selerio, J.E., Aro, J.L., Evangelista, S.S., et al., 2022. Optimal configuration of poly-generation plants under process failure, supply chain uncertainties, and emissions policies. Comput. Ind. Eng. 172, 108637. https://doi.org/10.1016/j.cie.2022.108637.
Shi, M.X., Li, L.T., Shao, D.J., et al., 2025. Coordinated source–network–storage inertia control strategy based on wind power transmission via MMC-HVDC system. Energy Eng. J. Assoc. Energy Eng. 123 (1). https://doi.org/10.32604/ee.2025.069915.
Tong, K.L., Gong, J., Yue, D.J., et al., 2013. Stochastic programming approach to optimal design and operations of integrated hydrocarbon biofuel and petroleum supply chains. ACS Sustain. Chem. Eng. 2 (1), 49–61. https://doi.org/10.1021/sc400267t.
Tu, R.F., Jiao, Y.i., Qiu, R., et al., 2023. Energy saving and consumption reduction in the transportation of petroleum products: A pipeline pricing optimization perspective. Appl. Energy 342, 121135. https://doi.org/10.1016/j.apenergy.2023.121135.
Tu, R.F., Liu, C.Y., Shao, Q., et al., 2024. Pipeline sharing: Optimal design of downstream green ammonia supply systems integrating with multi-product pipelines. Renew. Energy 223, 120024. https://doi.org/10.1016/j.renene.2024.120024.
Xiong, X.Q., Xu, N., Xing, X.K., et al., 2025. Design of intelligent scheduling and optimization decision system for multi-source regional crude oil transportation and distribution system. Int. Commun. Heat Mass Tran. 164, 108881. https://doi.org/10.1016/j.icheatmasstransfer.2025.108881.
Zhang, T.W., Zhong, W.M., Liu, Y.R., et al., 2025a. Incorporating large-scale economic-environmental-energy coupling assessment and collaborative optimization into sustainable product footprint management: A graph-assisted life cycle energy efficiency enhancement approach. Energy Convers. Manag. 329, 119616. https://doi.org/10.1016/j.enconman.2025.119616.
Zhang, X., Fu, G.T., Liao, Q., et al., 2025b. Large-scale hydrogen supply chain vision with blended pipeline transportation of China. Renew. Energy 240, 122230. https://doi.org/10.1016/j.renene.2024.122230.